

3D-FEM Modeling of Macrosegregation in Solidification of Binary Alloys

Sylvain Gouttebroze, Victor D. Fachinotti, Michel Bellet, Hervé Combeau

▶ **To cite this version:**

Sylvain Gouttebroze, Victor D. Fachinotti, Michel Bellet, Hervé Combeau. 3D-FEM Modeling of Macrosegregation in Solidification of Binary Alloys. International Journal of Forming Processes, 2005, 8, p. 203-217. hal-00678503

HAL Id: hal-00678503

https://minesparis-psl.hal.science/hal-00678503

Submitted on 13 Mar 2012

HAL is a multi-disciplinary open access archive for the deposit and dissemination of scientific research documents, whether they are published or not. The documents may come from teaching and research institutions in France or abroad, or from public or private research centers.

L'archive ouverte pluridisciplinaire **HAL**, est destinée au dépôt et à la diffusion de documents scientifiques de niveau recherche, publiés ou non, émanant des établissements d'enseignement et de recherche français ou étrangers, des laboratoires publics ou privés.

Int. J. Forming Processes 8 (2005) 203-217

3D-FEM Modeling of Macrosegregation in Solidification of Binary Alloys

S. Gouttebroze* — V.D. Fachinotti* — M. Bellet* — H. Combeau**

** Centre de Mise en Forme des Matériaux (CEMEF), Ecole des Mines de Paris, UMR 7635 CNRS. BP 207, F06904 Sophia Antipolis Cedex, France*
sylvain.gouttebroze@ensmp.fr

** LSG2M, Ecole des Mines de Nancy, Parc de Saurupt, F54000 Nancy, France.

ABSTRACT: *The paper presents a three-dimensional coupled numerical solution of momentum, energy and solute conservation equations, for binary alloy solidification. The mushy zone is modelled as a porous medium, saturated in liquid, following Darcy's law. Microsegregation is governed either by lever rule or Scheil models. The resulting solute, momentum and energy transport equations are solved using the Streamline-Upwind Petrov/Galerkin method. All these equations are coupled but solved with a single staggered scheme. The full algorithm was implemented in the 3D finite element code THERCAST. Two applications cases are given: solidification of Sn-Pb and Pb-Sn alloys in a parallelepipedic cavity. Comparisons with experimental measurements and with two other simulation codes are made. Full 3D and pseudo-2D calculations are also compared. Finally the mesh size effect on the accuracy of the solution is discussed.*

KEY WORDS: *macrosegregation, alloy solidification, 3D finite element.*

1. Introduction

Macrosegregation is a critical problem in alloy solidification. This inhomogeneity in solute concentration at the scale of the product is due to the transport of solute at a macroscopic scale. In this paper, we consider only the transport of solute due to the thermo-solutal convection for which the driving force is mainly located in the mushy zone. In order to solve this problem, conservation equations over the whole part domain, including the mushy domain may be obtained using either the classical mixture theory (Bennon *et al.*, 1987; Prakash *et al.*, 1989) or spatial averaging techniques (Ni *et al.*, 1991; Ahmad *et al.*, 1997).

The main objective of the present work is the prediction of the macrosegregation pattern in a solidifying binary alloy. First we present the equations and the strategy adopted in THERCAST®, a three-dimensional finite-element code developed by CEMEF (Bellet *et al.*, 2004). The implementation of the mixture theory and the spatial averaging technique has been already presented (see Fachinotti *et al.*, 2003 for details). Then we focus on the evolution of THERCAST with the implementation of two classical microsegregation models (lever rule and Scheil) and the coupled resolution of energy, solute and momentum conservation equations. Also the introduction of the SUPG-PSPG formulation of the mechanical problem is presented.

The obtained results for two test cases (Hebditch *et al.*, 1974), will be compared to experimental measurements on sections, and to those of SOLID, a 2D finite-volume code (Combeau *et al.* ,1990) and also to those of CALCOSOFT (Desbiolles *et al.*, 2003), the only other 3D finite element macrosegregation simulation code found in the literature.

2. Resolution of conservation equations

The analysis of fluid flow, temperature and solute distribution in a solidifying material needs the coupled resolution of the equations stating the conservation of momentum, energy and solute.

2.1. *Main assumptions of the model*

The present model of binary alloy solidification assumes

- laminar, constant-viscosity, Newtonian flow in the liquid;
- solid and liquid phase densities are equal and constant ($\rho_l=\rho_s=\rho_0$), except in the buoyancy force term of the motion equation, where density depends on the temperature T and on the solute concentration in the liquid phase w_l according to the Boussinesq approximation:

$$\tilde{\rho} = \rho_0 \left[1 - \beta_T \left(T - T_{ref}\right) - \beta_w \left(w_l - w_l^{ref}\right)\right] \quad [1]$$

where β_T and β_w are the thermal and solutal expansion coefficients, respectively, and w_l is the concentration in the liquid phase. Note that in this case, mass and volume concentrations coincide.

– a saturated mixture, i.e.:

$$g_s + g_l = 1 \quad [2]$$

being g_s (resp. g_l) the solid (resp. liquid) fraction; like solute concentration, those phase fractions are either mass or volume fractions.

– rigid and fixed solid phase, corresponding to a columnar solidification.

– the mushy region is modelled as an isotropic porous medium whose permeability is defined by the Carman-Kozeny formula

$$K = \frac{\lambda_2^2 g_l^3}{180(1 - g_l)^2} \quad [3]$$

where λ_2 is the secondary dendrite arms spacing.

– local thermodynamic equilibrium at the interface between liquid and solid phases

$$w_s^* = k w_l^* \quad [4]$$

$$T = T_m + m w_l^* \quad [5]$$

where w_s^* (resp. w_l^*) is the solute content in the solid phase (resp. liquid) at the interface, k is the partition coefficient, T_m is the melting temperature, and m the liquidus slope (assumed constant).

We refer to (Voller *et al.*, 1989) for a discussion on the range of validity of these assumptions.

2.2. *Microsegregation model*

Equations [7] and [8] are obtained using the mixture theory. The mean concentration results from the integration over a representative volume of the concentration in the two phases (Bennon *et al.*, 1987).

$$w = g_s w_s + g_l w_l \quad [6]$$

where w is the mean concentration, w_l the average concentration in the liquid phase and w_s the average concentration in the solid phase.

Only two classical models are considered here: the lever rule and the Scheil model. The diffusion in the liquid at microscopic scale is considered as perfect for both models. The diffusion in the solid is perfect for lever rule, while there is no diffusion in the solid in Scheil model. This leads to a simple averaging equation for Lever rule, but for Scheil model it is necessary to take into account the solidification history because of the non-uniform solid concentration in the representative volume.

Lever rule: $w = g_s w_s + g_l w_l = \left(k + (1-k)g_l\right)w_l$ [7]

Scheil model: $w = g_s w_s + g_l w_l = \int_0^{g_s} k w_l^* dg + g_l w_l$ [8]

In the following applications, only the lever rule has been used because of its simplicity and also to compare with other codes.

2.3. *Momentum conservation*

As presented in a previous paper (Fachinotti *et al.*, 2003), the classical mixture theory (Bennon *et al.*, 1987; Prakash *et al.*, 1989) yields the following equation of motion:

$$\rho_0 \frac{d\mathbf{V}}{dt} = \nabla \cdot (\mu \nabla \mathbf{V}) - \nabla p + \tilde{\rho}\mathbf{g} - \frac{\mu}{K}\mathbf{V} \qquad [9]$$

where $\mathbf{V}$ and p are the unknown averaged velocity ($\mathbf{V}=g_l\mathbf{V_l}$) and the pressure field, respectively, μ is the dynamic viscosity and $\boldsymbol{g}$ is the gravity acceleration.

The time-discretised form of equation [9] is obtained using the Euler-backward finite-difference technique.

The spatial discretisation was originally carried out using mixed $P1^+/P1$ tetrahedral finite elements (Jaouen, 1998). Inside each element, the velocity is interpolated by a linear function enriched by a piece-wise linear bubble function, while the pressure is linear and continuous. Together with these elements, a ALE formulation is used, where the variables are updated by the upwind nodal technique (Bellet *et al.*, 2004) which includes a lagrangian transport of the variables.

In this paper we also test another formulation newly implemented in THERCAST. The SUPG-PSPG formulation, presented for finite element calculations by (Tezduyar *et al.*, 2000), is based on three stabilization coefficients: a SUPG coefficient (stream-upwind/Petrov-Galerkin), a PSPG coefficient (pressure-stabilizing/Petrov-Galerkin) and a LSIC coefficient (least-squares on incompressibility constraint).

This formulation leads to the following weak form equation:

$$\int_{\Omega}\left(\rho\frac{\partial \mathbf{v}}{\partial t}+\rho_0\nabla\cdot(\mathbf{v}\times\mathbf{v})-\nabla\cdot(\mu\nabla\mathbf{v})+\frac{\mu}{\mathrm{K}}\mathbf{v}-\tilde{\rho}\mathbf{g}\right)\cdot\mathbf{v}^{*}d\Omega+\int_{\Omega}p^{*}\nabla\cdot\mathbf{v}d\Omega$$
$$+\sum_{e=1}^{nelt}\int_{\Omega^e}\left(\rho_0\frac{\partial \mathbf{v}}{\partial t}+\rho_0\nabla\cdot(\mathbf{v}\times\mathbf{v})-\nabla\cdot(\mu\nabla\mathbf{v})+\frac{\mu}{\mathrm{K}}\mathbf{v}-\tilde{\rho}\mathbf{g}\right)\cdot\frac{1}{\rho}(\tau_{SUPG}\rho_0\mathbf{v}\cdot\nabla\mathbf{v}^{*}+\tau_{PSPG}\nabla p^{*})d\Omega \quad [10]$$
$$+\sum_{e=1}^{nelt}\int_{\Omega^e}\tau_{LSIC}\nabla\cdot\mathbf{v}^{*}\rho_0\nabla\cdot\mathbf{v}d\Omega=0$$

where $\mathbf{v}^*$ et p^* are the test functions (here equal to the interpolation functions), and τ_{SUPG} is the streamline-upwind coefficient, τ_{PSPG} the pressure-stabilizing coefficient, and τ_{LSIC} the least-square stabilization on the incompressibility constraint.

The SUPG-PSPG formulation demonstrates a good stability when increasing time step and a good accuracy.

2.4. *Mass conservation*

Regarding the above hypotheses, the mass conservation equation reduces to:

$$\nabla\cdot\mathbf{V}=0 \quad [11]$$

where $\boldsymbol{V}$ is the averaged velocity of the liquid phase.

2.5. *Solute conservation*

Redistribution of solute is governed by the equation

$$\frac{\partial w}{\partial t}+\mathbf{V}\cdot\nabla w_l-\nabla\cdot(\varepsilon\nabla w)=0 \quad [12]$$

where w is the average solute concentration and ε is a diffusion coefficient, usually negligible but necessary for numerical purposes. For this reason the diffusion term can be expressed in terms of w instead of w_l as usual.

Following (Voller *et al.* ,1989), the time-integrated version of equation [12] is written as:

$$\frac{w-w^0}{\Delta t}+\mathbf{V}\cdot\nabla w-\nabla\cdot(\varepsilon\nabla w)=\mathbf{V}\cdot\nabla\left(w^0-w_l^0\right) \quad [13]$$

The superscript 0 refers to the values at the previous time step $t_0=t-\Delta t$. The discretized form of the advection term is split to avoid a non-linear resolution as presented by (Voller *et al.* ,1989).

The weak form of equation [13] is solved using the well-known Streamline Upwind/Petrov-Galerkin finite element method (Brooks *et al.*, 1982), with linear tetrahedral elements.

2.6. *Energy conservation*

We have implemented an enthalpy-based heat transfer model, which is governed by the energy balance equation written in the form

$$\frac{\partial h}{\partial t} + \mathbf{V} \cdot \nabla\left(\rho_0 c_p T\right) - \nabla \cdot \left(\kappa \nabla T\right) = 0 \qquad [14]$$

where κ is the thermal conductivity. According to the above mentioned hypotheses, the temperature T is related to the average volumic enthalpy h by the following equation:

$$h = \int_{T_0}^{T} \rho_0 c_p d\tau + \rho_0 g_l L \qquad [15]$$

where c_p and L are the material specific heat and latent heat of fusion, respectively.

Linear tetrahedral finite elements are used to discretise equation [14] in the spatial domain, while the Euler-backward finite difference technique is applied for time integration. The above-mentioned SUPG method is used for solving the advection-diffusion equation [14]. The eutectic transformation causes a jump in h(T) function. This non-linearity is treated using a Newton-Raphson algorithm.

2.7. *Resolution strategy*

The resolution is based on a weak coupling of the four equations. During a time increment, the resolution procedure is described by five steps:

1- Resolution of energy conservation (eventually with a time step optimization based on a maximal temperature increment per time step) to obtain the average mixture enthalpy h

2- Resolution of solute conservation equation to obtain the average mixture concentration w

3- Knowing w and h, the dependent nodal variables g_l, T, w_l are computed locally according to the adopted microsegregation model.

4- Resolution of momentum conservation equation to obtain the average mixture velocity **V** and the pressure *p*.

5- Updating of all the variables

Additional steps are necessary in case of remeshing, because in this case, a transport of the variables to the new positions of nodes is necessary.

In this work, this explicit staggered scheme is used for coupling the equations, which means that each equation is solved once time per time step because the full coupling of these equations leads to a prohibitive calculation time.

3. APPLICATION

The application cases consist of the solidification of Pb-48wt%Sn and Sn-5wt%Pb ingots studied by (Hebditch *et al.*, 1974). The phase diagram of lead-tin binary alloys is presented in Figure 1. In this test, the alloys are solidified in a parallelepipedic cavity (6 cm high, 10 cm wide and 1.3 cm thick, see Figure 2), which is insulated on all sides excepted the vertical side on the left. The position of the sections used for experimental measurements is also indicated in Figure 2.

3.1. *Sn-5%wtPb alloy*

The material and physical data are presented in Table 1. The computation has been performed with a non-structured mesh (29245 tetrahedral elements) refined at the walls. This case is considered as pseudo-2D by imposing two planes of symmetry and using only one element in the thickness in order to compare THERCAST results to those of the 2D code SOLID. A constant time step of 0.05s has been adopted. Figure 3 shows that the development of segregated channels in the mushy zone is similar with the two codes SOLID and THERCAST.

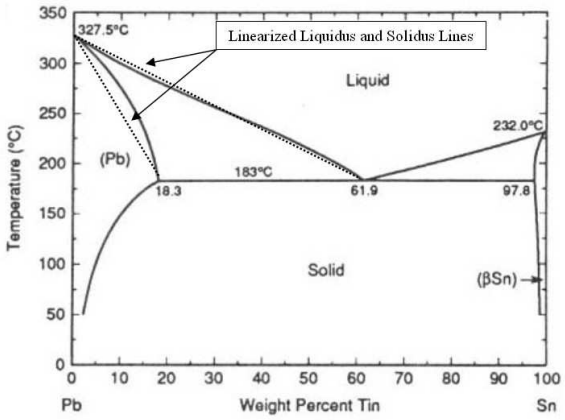


Figure 1. *Phase diagram of the Pb-Sn alloy*

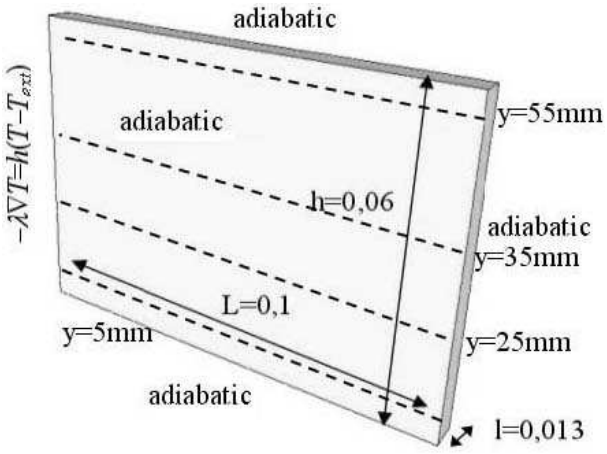
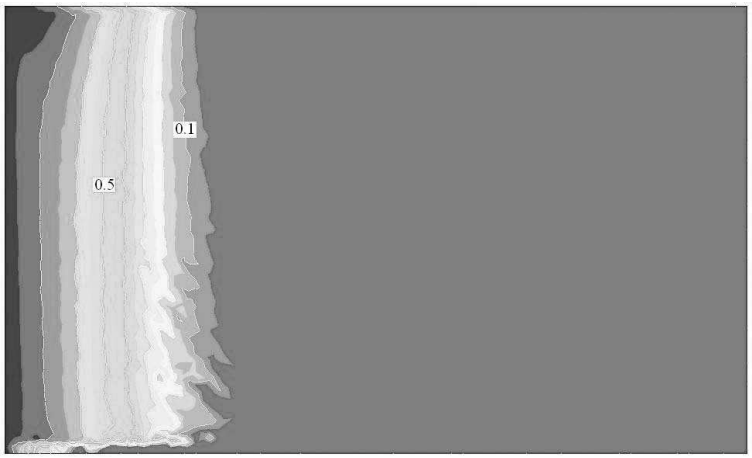


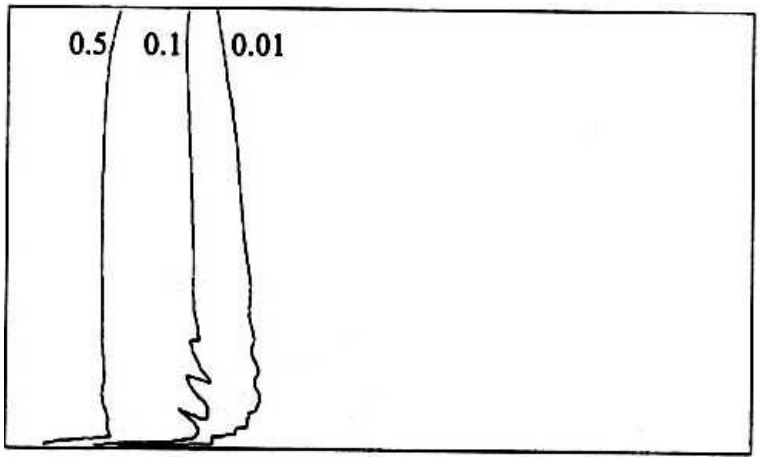
Figure 2. *Hebditch-Hunt test problem*

Thermal Conductivity λ	55 W m^{-1} K^{-1}	Initial Temperature T_{init}	226 °C
Specific Heat c_p	260 J kg^{-1} K^{-1}	Initial Concentration w_0	5 wt%
Latent Heat of Fusion L	61×10^3 J kg^{-1}	Reference Density ρ_0	7000 kg m^{-3}
Melt Temperature T_m	232 °C	Dynamic Viscosity μ	10^{-3} Pa s
Liquidus Line Slope m	-1.286 K $(wt\%)^{-1}$	Secondary Dendrite Arm Spacing λ_2	65 µm
Partition Coefficient k	0.0656	Heat Convection Coefficient h	300 W m^{-2} K^{-1}
Eutectic temperature	183 °C	Thermal Expansion Coefficient β_T	$0.6.10^{-4}$ K^{-1}
External Temperature T_{ext}	25 °C	Solutal Expansion Coefficient β_w	$-5.3\ 10^{-3}$ $(wt\%)^{-1}$
		Solutal Diffusivity ε	3.10^{-9} m^2 s^{-1}

Table 1. *Material and physical properties for Sn-5%wtPb case.*



a) THERCAST, FEM 3D



b) SOLID (Ahmad *et al.*, 1997), FVM 2D

Figure 3. *Comparison of solid fraction for Sn-5wt%Pb at 100s*

Such segregated channels lead to a destabilization of the solidification front (see Figure 4). In those channels, the solidification is delayed due to the liquid enrichment, which increases the permeability and consequently gives rise to higher velocities. Then, those regions show high solute, liquid fraction and velocity gradients. The accuracy of the calculation is then highly conditioned by the local mesh size.

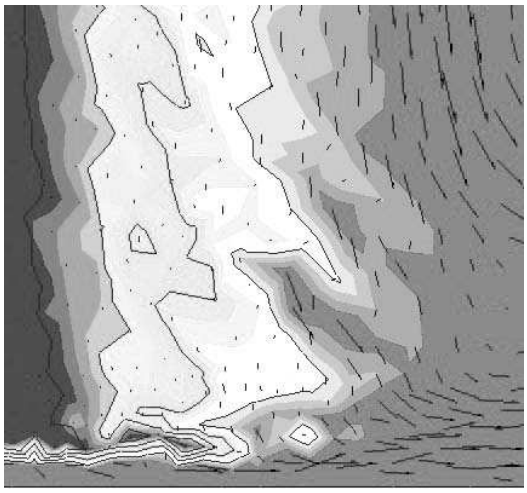


Figure 4. *Zoom on the solidification front for Sn-5wt%Pb at 100s with THERCAST*

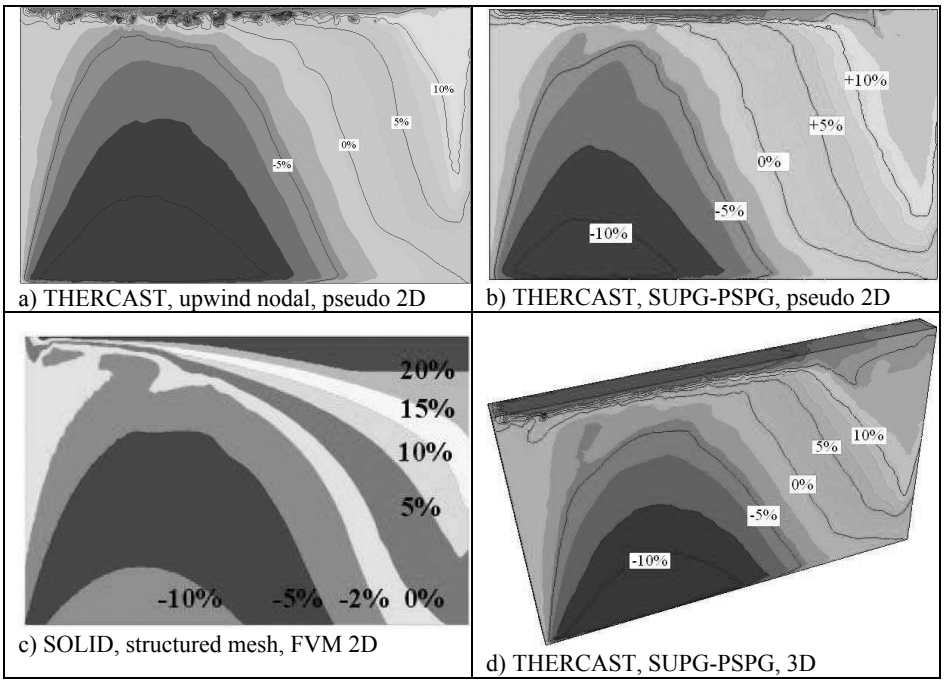
3.2. *Pb-48wt%Sn alloy*

The material and physical data are presented in Table 2. This computation is carried out with the same mesh as the previous alloy for pseudo-2D simulations but using a variable time step. The time step varies to limit the incremental temperature variation between 2 and 5°C. This technique leads to an optimized time step and a shorter computation time. In this case we also compare the two resolutions of the momentum equation: the upwind nodal formulation (Jaouen, 1998) and the SUPG-PSPG formulation.

Also a full 3D simulation has been done for this case. The mesh density is similar as the previous pseudo-2D case. The time step is adapted throughout the computation using the same technique as before. The calculation for the full 3D case is made using only the SUPG-PSPG formulation.

Thermal Conductivity λ	50 W m^{-1} K^{-1}	Initial Temperature T_{init}	216 °C
Specific Heat c_p	200 J kg^{-1} K^{-1}	Initial Concentration w_0	48 wt%
Latent Heat of Fusion L	53.55×10^3 J kg^{-1}	Reference Density ρ_0	9000 kg m^{-3}
Melt Temperature T_m	327.5 °C	Dynamic Viscosity μ	10^{-3} Pa s
Liquidus Line Slope m	-2.334 K $(wt\%)^{-1}$	Secondary Dendrite Arm Spacing λ_2	40 µm
Partition Coefficient k	0.307	Heat Convection Coefficient h	400 W m^{-2} K^{-1}
Eutectic temperature	183 °C	Thermal Expansion Coefficient β_T	10^{-4} K^{-1}
External Temperature T_{ext}	25 °C	Solutal Expansion Coefficient β_w	$4.5\ 10^{-3}$ $(wt\%)^{-1}$
		Solutal Diffusivity ε	10^{-9} m^2 s^{-1}

Table 2. *Material and physical properties for Pb-48%wtSn case.*



a) THERCAST, upwind nodal, pseudo 2D

b) THERCAST, SUPG-PSPG, pseudo 2D

c) SOLID, structured mesh, FVM 2D

d) THERCAST, SUPG-PSPG, 3D

Figure 5. *Comparison of average concentration for Pb-48wt%Sn alloy at 400s (labels on isolines indicate the relative variation with respect to the initial concentration, in percent)*

3.2.1. Comparison of the results

From Figure 5, it can be seen that the average concentration pattern at 400 s is close to the one calculated with SOLID. But at the top of the cavity, some wiggles appear in the channel of enriched liquid when using the upwind nodal formulation. This problem seems to perturb only locally the solution. These wiggles do not appear when the SUPG-PSPG formulation is used on both pseudo-2D and 3D calculations. These two calculations are in very good agreement. So we can deduce that the three-dimensional effects are negligible in this configuration. This result validates the calculation on such pseudo-2D geometries, when it is possible, in order to decrease the computation time. Compared to SOLID, the THERCAST results show a smaller region of high positive segregation at the top of the ingot. In THERCAST the level +20% is only reached in the liquid channel at the top. In the positive segregation area the solute concentration is also less stratified compared to SOLID results. This lower segregation is certainly caused by a stronger flow field in the liquid bulk during the solidification.

At the end of the solidification, THERCAST results are in good agreement with SOLID and CALCOSOFT results (Desbiolles *et al.*, 2003) and also with experimental data. In Figure 6, the results in the three lower sections are close to the experimental measurements except near the right wall in the 25mm section. On the contrary, in top section (near the liquid channel), some discrepancy in the results has been found. As previously shown, the positive segregation predicted by THERCAST is lower than experimental data which is even clearer on the 55mm section. This point needs to be investigated to better predict the end of the solidification. Moreover these results should be improved by taking into account the ingot deformation in the models.

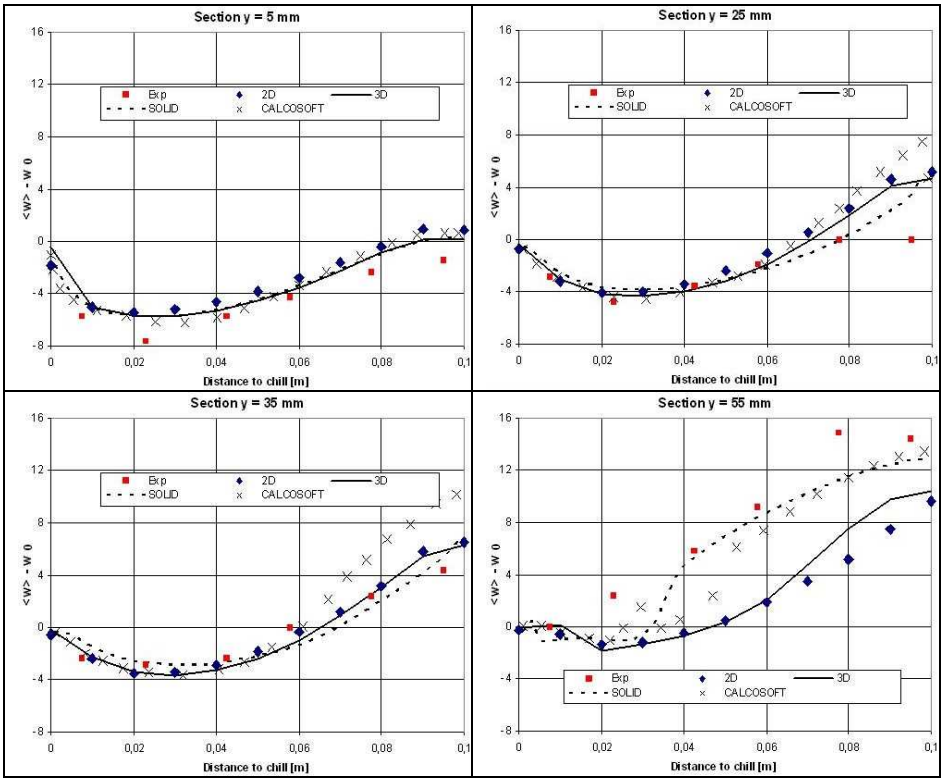


Figure 6. *Macrosegregation on four horizontal sections at the end of solidification for the Pb-48wt%Sn alloy*

3.2.2. Effect of the mesh size on the prediction of macrosegregation

In this last section, we would like to illustrate the mesh effect on the macrosegregation calculation by studying the formation of the solidification front in the top left corner of the cavity for pseudo-2D meshes at time 10s. We have seen

that for the first calculation made with the upwind nodal approach this area presented oscillations for the mean concentration in solute. So it seems important to better understand how and why this problem occured.

Three different meshes with increasing refinement have been selected. The first mesh (16331 nodes, 47731 elements) is refined near all the walls and coarse in the center part. The second mesh (18986 nodes, 55710 elements) is similar but the top part of the left corner (where the liquid channel appear) is finer. The last mesh (112699 nodes, 336078 elements) is highly refined particularly in the top part.

A zoom, corresponding to the region at the top left corner of the meshes, the liquid fraction and the mean concentration in solute at time 10s are presented in Figure 7.

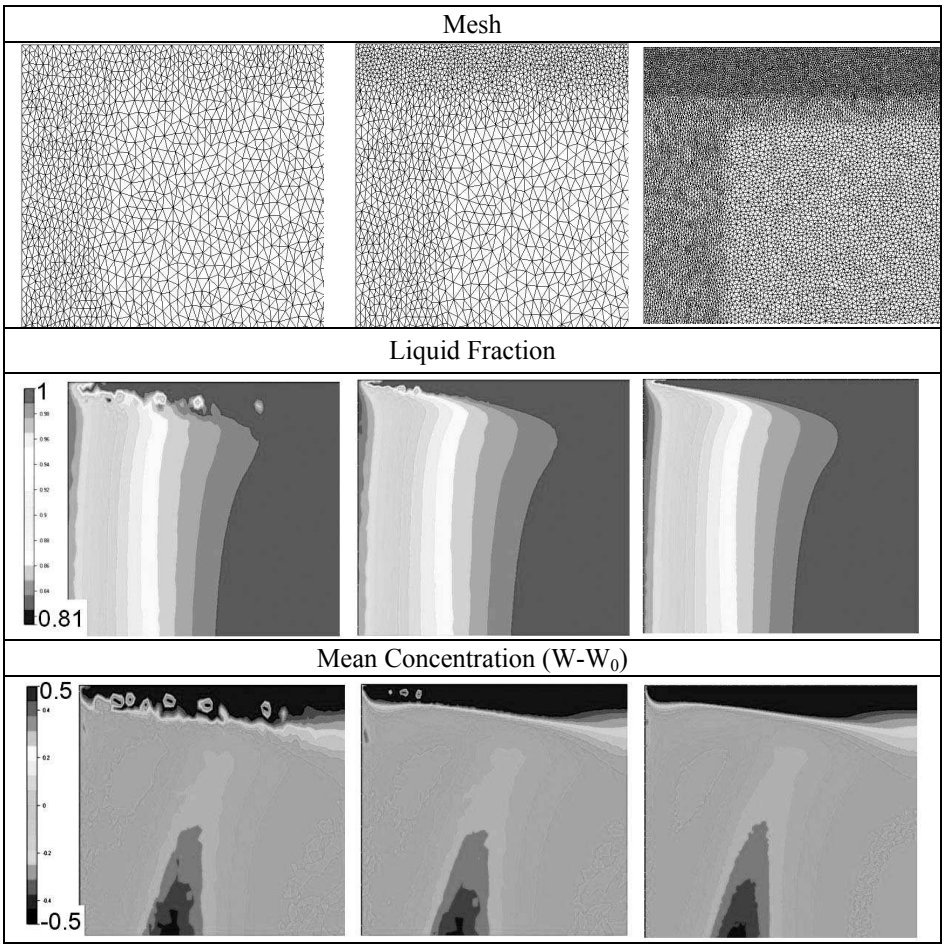


Figure 7. *Liquid fraction and mean concentration at 10s for the Pb-48wt%Sn alloy on three different meshes*

These results clearly show that the irregularities previously described come from the coarseness of the mesh. We can also deduce that such problems can be avoided by using a mesh highly refined everywhere since interface moves all along the computation. It will then lead to a huge calculation time. An efficient solution would be to adapt automatically the local mesh density during the calculation.

4. Conclusions

A 3D FEM modeling of macrosegregation has been presented and implemented in the solidification code THERCAST. The solidification simulation of a Sn-5%wtPb alloy shows that THERCAST seems able to predict channel formation and the associated macrosegregation. The application cases show good agreement with both experimental measurements and SOLID results. THERCAST has been also successfully compared with CALCOSOFT, a 3D finite element code.

The 3D and pseudo-2D approaches show good agreement in the Pb-48%Sn case, which validates the use of pseudo-2D simulations for similar geometries. The study of the mesh influence then demonstrates a strong link between irregularties in the solution and the mesh size in critical areas of high liquid fraction gradient.

THERCAST provides a useful tool for the study of macrosegregation in three-dimensional solidification of binary alloys.

In the future, a more accurate resolution is needed in the channel where complex flow field takes place due to important gradients of liquid fraction and permeability. This should lead us to develop an adaptive remeshing strategy in order to increase the accuracy in these particular areas.

Acknowledgements

This work has been supported by the French Ministry of Industry, the French Technical Center of Casting Industries (CTIF) and the companies Arcelor, Ascometal, Fonderie de l'Atlantique, Aubert et Duval, Erasteel, Industeel and PSA. V.D. Fachinotti has taken part in this study during his post-doctoral stay in Cemef, granted by the Argentine Council for Scientific and Technical Research (CONICET).

References

Ahmad N., Combeau H., Desbiolles J.-L., Jalanti T., Lesoult G., Rappaz M., Stomp C., "Numerical Simulation of Macrosegregation: a Comparison between Finite Volume

Method and Finite Element Method Predictions and a Confrontation with Experiments", *Metall. and Mat. Trans.* 29A (1997) 617-630.

Bellet M., Fachinotti V.D., "ALE method for solidification modelling", *Comput. Methods Appl. Mech. Engrg.* 193 (2004) 4355-4381

Bennon W.D., Incropera F.P., "A Continuum Model for Momentum, Heat and Species Transport in Binary Solid-Liquid Phase Change Systems – I. Model Formulation", *Int. J. Heat Mass Transfer* 30 (1987) 2161-2170.

Brooks A.N., Hughes T.J.R., "Streamline Upwind/Petrov-Galerkin Formulations for Convection Dominated Flows with Particular Emphasis on the Incompressible Navier-Stokes Equations", *Comput. Methods Appl. Mech. Engrg.* 32 (1982) 199-259.

Combeau H., Roch F., Chevrier J. C., Poitrault I., Lesoult G., "Numerical Study of Heat and Mass Transfer during Solidification of Steel Ingots", In: *Advanced Computational Methods in Heat Transfer*, ed. L. C. Wrobel, Springer-Verlag, New York (1990) 79-90.

Desbiolles J.-L., Thevoz Ph., Rappaz M., "Micro-/Macrosegregation modeling in casting: a fully coupled 3D model*". Proceedings of Modeling of Casting, Welding and Advanced Solidification Processes X, TMS*, 2003, p.245-252.

Fachinotti V.D., Bellet M., "Three Dimensional Finite Element Modelling of Thermomechanics and Macrosegregation in Binary Alloys Solidification", *Sixth ESAFORM Conference*, Salerno, April 28-30, 2003

Hebditch D.J., Hunt J.D., "Observations of Ingot Macrosegregation on Model Systems". *Metall. Trans*. 5 (1974) 1557-1564.

Jaouen O., Modélisation Tridimensionnelle par Eléments Finis pour l'Analyse Thermo-Mécanique du Refroidissement des Pièces Coulées, PhD Thesis, Ecole des Mines de Paris (1998).

Ni J., Beckermann C., "A Volume-Averaged Two-Phase Model for Transport Phenomena during Solidification", *Metall. Trans.* 22B (1991) 349-361.

Prakash C., Voller V., "On the Numerical Solution of Continuum Mixture Equations Describing Binary Solid-Liquid Phase Change", *Num. Heat Transfer B* 15 (1989) 171-189.

Tezduyar T.E., Osawa Y., "Finite element stabilization parameters computed from element matrices and vectors", *Comput. Methods Appl. Mech. Engrg.* 190(2000), p.411-430.

Voller V.R., Brent A.D., Prakash C., "The Modelling of Heat, Mass and Solute Transport in Solidification Systems", *Int. J. Heat Mass Transfer* 32 (1989) 1719-1731.